JOURNAL OF AIRCRAFT
Vol. 32, No. 5, September–October 1995

Evaluation of Blockage Interference on Propellers in a Perforated-Wall Wind Tunnel

M. Mokry*
National Research Council of Canada, Ottawa K1A 0R6, Canada

A method for the evaluation of blockage interference for propeller models in a perforated-wall wind tunnel is presented. The correction procedure, based on a Fourier solution for the Dirichlet problem inside a cylindrical flow domain, uses boundary data obtained from pressure measurements along the wind-tunnel walls and a far-field representation of the propeller. The radial contraction of the slip stream is modeled by a sink, whose strength and location are evaluated from the measured thrust and power using axial momentum theory. An iterative procedure is developed for a compressible slip stream, using the Rankine–Froude theory as the first approximation. The equations describing the discontinuity of momentum and energy across the propeller disk are discussed and solved similarly to those describing a discontinuity across a normal shock.

Nomenclature

A = slip-stream cross-sectional area, $\pi D^2/4$
A_w = wind-tunnel cross-sectional area
a_n, b_n = Fourier components of u
$\hat{a}_n$, $\hat{b}_n$ = boundary values of a_n, b_n
C_P = power coefficient, $P/(\rho_0 N^3 D_p^5)$
C_p = pressure coefficient
C_T = thrust coefficient, $T/(\rho_0 N^2 D_p^4)$
c = velocity of sound
D = slip-stream diameter
D_n = differential operator
$F_{n,k}$ = coefficient of Fourier sine series
f_n = common notation for a_n and b_n
$\hat{f}_n$ = common notation for $\hat{a}_n$ and $\hat{b}_n$
I_n = modified Bessel function of the first kind of order n
i = enthalpy
J_n = Bessel function of the first kind of order n
J_0 = advance ratio, v_0/ND_p
j = mass flux density, ρv
$j_{n,k}$ = kth positive zero of J_n
M = Mach number
m = integer power of 2, number of subdivisions of interval $2s$
N = propeller rotational speed, rps
P = power
$P_{n,k}$, $Q_{n,k}$ = coefficients of Fourier–Bessel series
R = slip-stream radius or gas constant
r = radius of control cylinder
r, Θ = polar coordinates in the transformed space
s = reduced test section length or entropy
T = thrust
u = axial component of wall interference velocity
v = axial velocity
x, ρ, θ = cylindrical coordinates
β = Prandtl–Glauert factor, $\sqrt{1 - M_0^2}$
γ = ratio of specific heats, 1.4
ΔM = Mach number correction
η = propeller efficiency
μ_k, $\nu_{n,k}$ = eigenvalues
ν = thrust-power term
ξ = transformed axial coordinate
ρ = air density
σ = strength of sink representing propeller far field
τ = modified thrust coefficient, $4C_T/(\pi J_0^2)$
ϕ = velocity potential
φ = disturbance velocity potential
φ_f = free air part of φ
φ_w = wall interference part of φ
ψ = stream function
Ω = area ratio, A_0/A_3

Subscripts
id = ideal
n = index of the Fourier component
p = propeller
0 = station far upstream
1 = station immediately ahead of propeller plane
2 = station immediately behind propeller plane
3 = station far downstream
* = critical

Introduction

IN the past two decades, advanced high-speed propellers have been found to offer significant fuel savings and associated operating cost benefits for aircraft cruising in the Mach 0.7–0.8 speed range. The wind-tunnel testing has, understandably, played an important role in the evaluation of the propulsive efficiency and optimization of this new generation of propellers.

Wall interference has been identified,[1] together with model support interference and scale effects, as one of the factors adversely affecting the reliability of wind-tunnel test data. Unfortunately, Glauert's correction technique,[2] based on the axial momentum balance, cannot be easily extended to ventilated-wall wind tunnels where most of the high-speed testing is currently being done.

One can, however, utilize the well-established one-component correction method,[3–5] which does not require the knowledge of mass and momentum transfer through the walls. The boundary values of the streamwise component of wall interference velocity are obtained from static pressure measurements near the test section walls and the estimated far field of the model in free air. For perforated test section walls,

Presented as Paper ICAS-94-3.2.1 at the 19th Congress of the International Council of Aeronautical Sciences, Anaheim, CA, Sept. 18–23, 1994; received October 23, 1994; revision received April 10, 1995; accepted for publication April 13, 1995.

*Senior Research Officer, Institute for Aerospace Research, High Speed Aerodynamics Laboratory. Member AIAA.

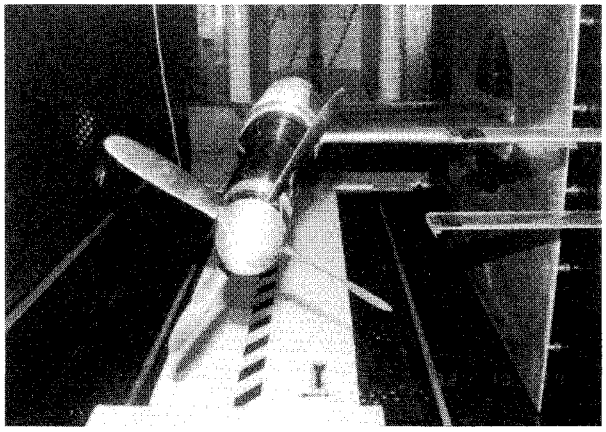

Fig. 1 Propeller test rig and static pressure tubes in the IAR 1.5 × 1.5 m wind tunnel (courtesy of de Havilland, Inc.).

suitable pressure-measuring devices are cylindrical tubes equipped with static pressure orifices facing the test section interior, in the direction normal to the wall. In Fig. 1, showing the experimental setup in the Institute for Aerospace Research (IAR) 1.5 × 1.5 m test section, three out of a total of six installed tubes can be seen: two at the bottom (on each side of the removable floor board) and one on the sidewall.

Using model geometry and the measured lift force, the far-field effects of a nacelle and a wing in subsonic flow can be represented in the usual fashion by sources, sinks, and horseshoe vortices. The steady part of the propeller far field, which is due to the radial contraction of the propulsive stream tube, can be represented by a sink, whose strength and location are evaluated from the measured thrust and power using the axial momentum theory.

The far-field representation becomes unnecessary in the two-component approach,[6] where both the static pressure and flow angle distributions are measured around the test section boundary. The penalty, compared to the one-variable method, is the added difficulty of making the measurement of flow angle in the highly perturbed environment of the ventilated walls.[7]

Correction Method

The flow is investigated in the cylindrical domain $x_1 < x < x_2$, $0 \le \rho < r$, $0 \le \theta < 2\pi$, inscribed in the wind-tunnel test section. As indicated in Fig. 2, r is the radius and x_1 and x_2 are the upstream and downstream ends of the domain, respectively. It is assumed that flow near the boundary is subsonic and that the disturbance velocity potential $\varphi(x, \rho, \theta)$ satisfies the linearized equation

$$\beta^2 \frac{\partial^2 \varphi}{\partial x^2} + \frac{1}{\rho}\frac{\partial}{\partial \rho}\left(\rho \frac{\partial \varphi}{\partial \rho}\right) + \frac{1}{\rho^2}\frac{\partial^2 \varphi}{\partial \theta^2} = 0 \tag{1}$$

According to small disturbance theory, the pressure coefficient at $\rho = r$ is obtained as

$$C_p(x, r, \theta) = -2\frac{\partial \varphi}{\partial x}(x, r, \theta) \tag{2}$$

Within the linearized flow region we apply the decomposition

$$\varphi(x, \rho, \theta) = \varphi_f(x, \rho, \theta) + \varphi_w(x, \rho, \theta) \tag{3}$$

where φ_f is the disturbance velocity potential due to the model in free air and φ_w is the wall interference potential. Using the scaled coordinate

$$\xi = (1/\beta)(x - x_1) \tag{4}$$

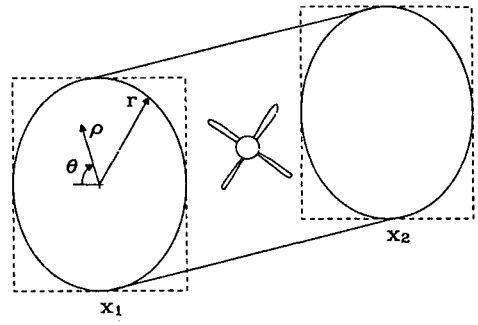

Fig. 2 Cylindrical flow domain.

we introduce the transformed axial component of wall interference velocity

$$u(\xi, \rho, \theta) = \frac{\partial \varphi_w}{\partial \xi}(x, \rho, \theta) = \beta \frac{\partial \varphi_w}{\partial x}(x, \rho, \theta) \tag{5}$$

Differentiation of Eq. (1) with respect to ξ and substitution from Eqs. (3) and (5) provide the governing equation

$$\frac{\partial^2 u}{\partial \xi^2} + \frac{1}{\rho}\frac{\partial}{\partial \rho}\left(\rho \frac{\partial u}{\partial \rho}\right) + \frac{1}{\rho^2}\frac{\partial^2 u}{\partial \theta^2} = 0 \tag{6}$$

in the domain $0 < \xi < s$, $0 \le \rho < r$, $0 \le \theta < 2\pi$, where

$$s = (1/\beta)(x_2 - x_1) \tag{7}$$

The boundary values are obtained from Eqs. (2–5) as

$$u(\xi, r, \theta) = -\beta\left[\frac{1}{2}C_p(x, r, \theta) + \frac{\partial \varphi_f}{\partial x}(x, r, \theta)\right] \tag{8}$$

where C_p is obtained by measurement and φ_f is expected to be known. Since r = constant, locations of the pressure measuring tubes are specified only by the azimuthal angles θ. There is no easy correction to the input value $u(\xi, r, \theta)$ should the actual radial coordinate of the tube differ from r.

Using periodicity, the solution is constructed in terms of the Fourier series

$$u(\xi, \rho, \theta) = a_0(\xi, \rho) + \sum_{n=1}^{\infty}[a_n(\xi, \rho)\cos n\theta + b_n(\xi, \rho)\sin n\theta] \tag{9}$$

Substitution in Eq. (6) gives

$$\begin{aligned} D_n a_n(\xi, \rho) &= 0, \qquad n = 0, 1, 2, \ldots \\ D_n b_n(\xi, \rho) &= 0, \qquad n = 1, 2, \ldots \end{aligned} \tag{10}$$

where

$$D_n = \frac{\partial^2}{\partial \xi^2} + \frac{\partial^2}{\partial \rho^2} + \frac{1}{\rho}\frac{\partial}{\partial \rho} - \frac{n^2}{\rho^2} \tag{11}$$

In order to solve for the Fourier components a_n and b_n, we introduce the boundary values

$$\begin{aligned} \hat{a}_n(\xi) &= a_n(\xi, r) \\ \hat{b}_n(\xi) &= b_n(\xi, r) \end{aligned} \tag{12}$$

and express them, using Eq. (9), in terms of the known values $u(\xi, r, \theta)$. The actual number of Fourier components we are able to exploit is given by the number of pressure measuring tubes (typically 4–6).

Using Eqs. (10) and (12), and f_n as a common notation for both a_n and b_n, we can set up the following Dirichlet boundary value problem:

$$\begin{aligned} D_n f_n(\xi, \rho) &= 0, \qquad 0 < \xi < s, \qquad 0 \le \rho < r \\ f_n(\xi, r) &= \hat{f}_n(\xi), \qquad 0 \le \xi \le s \\ f_n(0, \rho) &= \hat{f}_n(0)(\rho/r)^n, \qquad 0 \le \rho \le r \\ f_n(s, \rho) &= \hat{f}_n(s)(\rho/r)^n, \qquad 0 \le \rho \le r \end{aligned} \tag{13}$$

The last two boundary conditions, which were added on the upstream and downstream surfaces in order to complete the specification of the Dirichlet problem, were formulated so as to ensure close-form solutions for the coefficients of the resulting Fourier–Bessel series.

Applying the method of separation of variables (see the Appendix), the solution is obtained in terms of the Fourier sine series in ξ and the Fourier–Bessel series in ρ:

$$\begin{aligned} f_n(\xi, \rho) &= \sum_{k=1}^{\infty} F_{n,k} \frac{I_n(\mu_k \rho)}{I_n(\mu_k r)} \sin \mu_k \xi \\ &+ \sum_{k=1}^{\infty} \left[P_{n,k} \frac{\sinh \nu_{n,k}(s - \xi)}{\sinh \nu_{n,k} s} + Q_{n,k} \frac{\sinh \nu_{n,k} \xi}{\sinh \nu_{n,k} s} \right] \\ &\times J_n(\nu_{n,k} \rho) \end{aligned} \tag{14}$$

The eigenvalues entering Eq. (14) are

$$\mu_k = k\pi/s \quad \text{and} \quad \nu_{n,k} = j_{n,k}/r \tag{15}$$

where $j_{n,k}$ is the kth positive root of J_n.

The boundary values are contained in the coefficients

$$F_{n,k} = \frac{2}{s} \int_0^s \hat{f}_n(\xi) \sin \mu_k \xi \, d\xi \tag{16}$$

$$\begin{aligned} P_{n,k} &= \frac{2}{r^2 J_{n+1}^2(\nu_{n,k} r)} \int_0^r \hat{f}_n(0) \left(\frac{\rho}{r} \right)^n J_n(\nu_{n,k} \rho) \rho \, d\rho \\ &= \frac{2}{\nu_{n,k} r J_{n+1}(\nu_{n,k} r)} \hat{f}_n(0) \\ Q_{n,k} &= \frac{2}{\nu_{n,k} r J_{n+1}(\nu_{n,k} r)} \hat{f}_n(s) \end{aligned} \tag{17}$$

The coefficients $F_{n,k}$ can be evaluated[8] by the fast Fourier transform (FFT):

$$\begin{aligned} F_{n,k} &= \frac{2}{m} \sum_{j=0}^{m-1} \hat{f}_n \left(s \frac{2j + 1}{m} \right) \sin \frac{2\pi jk}{m} \\ k &= 1, 2, \ldots, m/2 - 1 \end{aligned} \tag{18}$$

where m is an integer power of 2 and the discrete values of $\hat{f}_n$ are obtained using the odd extension of the boundary function $\hat{f}_n(\xi)$ on the interval $0 \le \xi < 2s$. Accordingly, the Fourier sine series is truncated to the first $m/2 - 1$ terms. For the sake of notational convenience, the same number of terms is also used for the truncated Fourier–Bessel series.

On the wind-tunnel axis, $\rho = 0$, we obtain from Eqs. (9), (14), (16), and (17)

$$\begin{aligned} u(\xi, 0, \theta) &= \sum_{k=1}^{m/2-1} A_{0,k} \frac{\sin \mu_k \xi}{I_0(\mu_k r)} \\ &+ \sum_{k=1}^{m/2-1} \left[\hat{a}_0(0) \frac{\sinh \nu_{0,k}(s - \xi)}{\sinh \nu_{0,k} s} + \hat{a}_0(s) \frac{\sinh \nu_{0,k} \xi}{\sinh \nu_{0,k} s} \right] \\ &\times \frac{2}{\nu_{0,k} r J_1(\nu_{0,k} r)} \end{aligned} \tag{19}$$

where, according to Eq. (18)

$$A_{0,k} = \frac{2}{m} \sum_{j=0}^{m-1} \hat{a}_0 \left(s \frac{2j + 1}{m} \right) \sin \frac{2\pi jk}{m} \tag{20}$$

Using the described procedure, the wall interference velocity can also be evaluated at an arbitrary interior point of the domain $0 < \xi < s$, $0 \le \rho < r$, $0 \le \theta < 2\pi$.

The local Mach number correction is obtained from the differential relationship between the Mach number and velocity:

$$\Delta M(x, r, \theta) = (1/\beta)\{1 + [(\gamma - 1)/2] M_0^2\} M_0 u(\xi, \rho, \theta) \tag{21}$$

Propeller Far Field

The steady, subsonic far field of the propeller is derived using the axial momentum theory. Figure 3 shows the four stations of the (propulsive) stream tube representing the propeller slip stream. Stations 1 and 2, respectively, are immediately ahead of and immediately behind the propeller. Stations 0 and 3, respectively, are far upstream and far downstream.

The assumptions of the one-dimensional axial-momentum theory are as follows:

1) The propeller is represented by an "actuator" disk, of the same diameter as the actual propeller, across which axial momentum is added to the slip stream.

2) The slip stream is confined within a stream tube of circular cross section, passing through the disk circumference and extending from upstream infinity to downstream infinity.

3) The velocity in this stream tube is uniform and the rotary motion is neglected.

4) The stream tube cross-sectional area is continuous across the disk, $A_1 = A_2 = A_p$.

5) Flow upstream and downstream of the disk is inviscid.

6) Far downstream, the static pressure in the wake returns to the freestream value, $p_3 = p_0$.

The efficiency of the propeller, defined as the propulsive work divided by the power input, can be expressed in terms of the propeller thrust and power, or the corresponding dimensionless coefficients, as

$$\eta = v_0 T/P = J_0 C_T/C_P \tag{22}$$

The far-field effect of the slip-stream contraction will be represented by a sink placed at the origin of the wind-tunnel coordinate system (Fig. 3). The propeller axis is assumed to coincide with the wind-tunnel axis, but the actual x coordinate of the propeller disk is not known at this stage. Using the scaled streamwise coordinate

$$\xi = x/\beta \tag{23}$$

the potential of the sink will be

$$\varphi_f = \sigma/(4\pi r) \tag{24}$$

where

$$r = \sqrt{\xi^2 + \rho^2} \tag{25}$$

is the distance from the sink in the transformed space.

A combination of the source [Eq. (24)] and a uniform flow normalized by freestream velocity v_0 is described by the velocity potential

$$\phi = \sigma/(4\pi r) + r \cos \Theta \tag{26}$$

where

$$\Theta = \arccos \xi/r \tag{27}$$

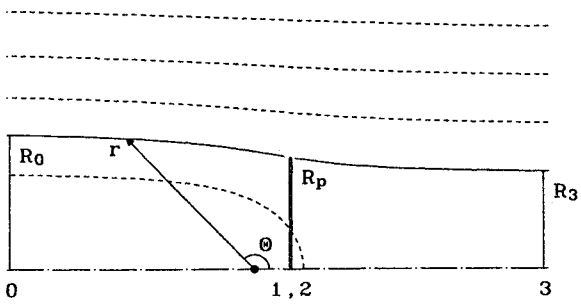

Fig. 3 Slip-stream boundary modeled by a sink.

The corresponding (Stokes') stream function is[9]

$$\psi = (\sigma/4\pi)\cos\Theta + \tfrac{1}{2}r^2\sin^2\Theta \tag{28}$$

Using Eq. (28), the slip-stream radius is

$$R = r\sin\Theta = \sqrt{2[\psi - (\sigma/4\pi)\cos\Theta]}, \qquad \psi > (\sigma/4\pi) \geq 0 \tag{29}$$

and the slip-stream cross-sectional area

$$A = \pi R^2 = 2\pi\psi - \tfrac{1}{2}\sigma\cos\Theta \tag{30}$$

Far upstream and downstream

$$\Theta = \pi, \qquad A = A_0 = 2\pi\psi + \tfrac{1}{2}\sigma \tag{31}$$

$$\Theta = 0, \qquad A = A_3 = 2\pi\psi - \tfrac{1}{2}\sigma \tag{32}$$

Adding and subtracting Eqs. (31) and (32), we obtain the values of the stream function defining the boundary of the slip stream

$$\psi = (1/4\pi)(A_0 + A_3) \tag{33}$$

and the sink strength

$$\sigma = A_0 - A_3 \tag{34}$$

Substituting Eqs. (33) and (34) in Eq. (30), we obtain for the propeller disk

$$\cos\Theta_p = \frac{A_0 + A_3 - 2A_p}{A_0 - A_3} \tag{35}$$

Taking into account Eq. (23), the axial coordinate of the propeller is then

$$x_p = \beta R_p \cot\Theta_p \tag{36}$$

Incompressible Slip stream

The balance of the mass flux, momentum, and energy provides the following set of equations[2] for the incompressible, inviscid flow inside the slip stream:

Station $0 \rightarrow 1$

$$A_0 v_0 = A_p v_1 \tag{37}$$

$$v_0^2/2 + p_0/\rho = v_1^2/2 + p_1/\rho \tag{38}$$

Station $1 \rightarrow 2$

$$v_1 = v_2 \tag{39}$$

$$p_1 + \rho v_1^2 + T/A_p = p_2 + \rho v_2^2 \tag{40}$$

Station $2 \rightarrow 3$

$$A_p v_2 = A_3 v_3 \tag{41}$$

$$v_2^2/2 + p_2/\rho = v_3^2/2 + p_3/\rho \tag{42}$$

Far-field conditions

$$p_3 = p_0 \tag{43}$$

$$T = A_p\rho v_1(v_3 - v_0) \tag{44}$$

Here, A_p, v_0, p_0, ρ, and T are expected to be known, and A_0, A_3, v_1, v_2, v_3, p_1, p_2, and p_3 are expected to be unknown.

From Eqs. (38–40) and (42) and (43)

$$T = A_p(p_2 - p_1) = \tfrac{1}{2}A_p\rho(v_3^2 - v_0^2) \tag{45}$$

and comparing it with Eq. (44) gives

$$v_1 = v_2 = \tfrac{1}{2}(v_0 + v_3) \tag{46}$$

both of them being well-known results from the Rankine–Froude theory.

Using continuity relationships, Eqs. (37), (39), and (41), we obtain for the area ratio

$$\Omega \equiv \frac{A_0}{A_3} = \frac{v_3}{v_0} = \sqrt{1 + \frac{v_3^2 - v_0^2}{v_0^2}} \tag{47}$$

and, from Eq. (45), in terms of thrust

$$\Omega = \sqrt{1 + \frac{T}{\frac{1}{2}A_p\rho v_0^2}} = \sqrt{1 + \frac{8}{\pi}\frac{C_T}{J_0^2}} \tag{48}$$

The power used in producing thrust is

$$P = \tfrac{1}{2}A_p\rho v_1(v_3^2 - v_0^2) = \tfrac{1}{2}(v_0 + v_3)T \tag{49}$$

Substituting Eq. (49) in Eq. (22) and using Eqs. (46) and (47), we obtain the ideal (Froude) efficiency in terms of Ω:

$$\eta_{id} = 2v_0/(v_0 + v_3) = 2/(1 + \Omega) \tag{50}$$

From Eqs. (37), (41), (46), and (47)

$$A_0/A_p = v_1/v_0 = \tfrac{1}{2}(1 + \Omega) \tag{51}$$

$$A_3/A_p = v_2/v_3 = \tfrac{1}{2}[1 + (1/\Omega)] \tag{52}$$

and, substituting in Eqs. (34–36)

$$\sigma = \tfrac{1}{2}[\Omega - (1/\Omega)]A_p \tag{53}$$

$$\cos\Theta_p = (\Omega - 1)/(\Omega + 1) \tag{54}$$

$$x_p = \tfrac{1}{2}[\sqrt{\Omega} - (1/\sqrt{\Omega})]R_p \tag{55}$$

For a positive thrust, $\Omega > 1$, we obtain $x_p > 0$, indicating that the propeller disk is downstream of the sink. Figure 4 shows that both σ/A_p and x_p/R_p increase as η_{id} decreases.

The obtained sink strength [Eq. (53)], can be readily used to estimate the velocity correction for a propeller inside a closed-wall wind tunnel. For an infinitely long, circular cross-sectional wind tunnel, the correction to (unit) stream velocity at a sink of strength σ on the tunnel axis is[10]

$$u = -\sigma/(2A_w) = -\tfrac{1}{4}[\Omega - (1/\Omega)](A_p/A_w)$$

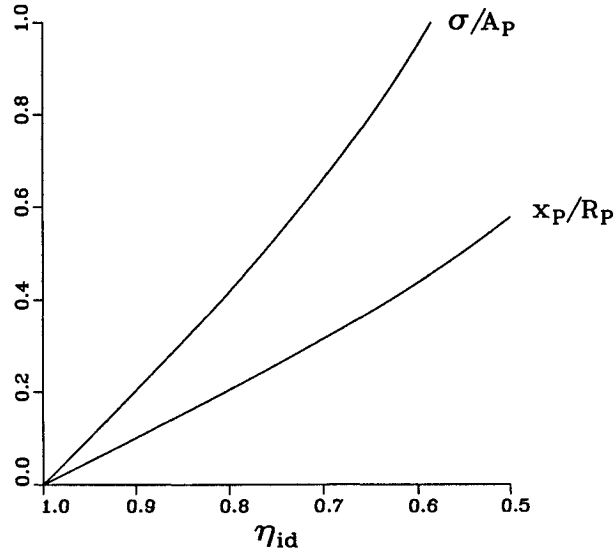

Fig. 4 Sink strength and propeller location for incompressible slip stream.

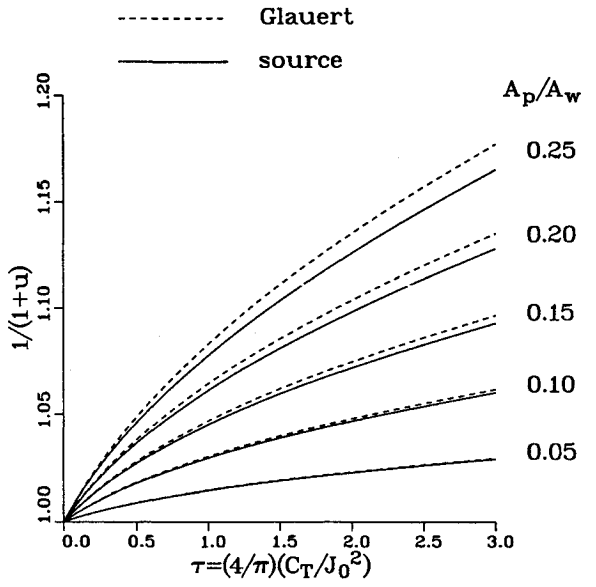

Fig. 5 Ratio of uncorrected and corrected stream velocities in a closed-wall wind tunnel.

Using Eq. (48), Ω can further be expressed in terms of thrust or its coefficient. In Fig. 5, the ratio of uncorrected and corrected stream velocities is plotted as a function of

$$\tau = \frac{T}{\rho A_p v_0^2} = \frac{4}{\pi}\frac{C_T}{J_0^2}$$

and compared with the successive approximation result by Glauert.[2] We see that there is a good agreement for small A_p/A_w, but the discrepancy becomes more apparent as the size of the propeller with respect to the wind tunnel increases. The source of this discrepancy is due to the fact that Glauert's correction technique[2] utilizes conservation of the axial momentum, whereas a correction method based on the sink representation is, in general, nonconservative. (The contraction of the slip stream in the wind tunnel is assumed the same as it would be in free air.) Unfortunately, the more rigorous method of Glauert cannot be extended to ventilated-wall wind tunnels, where transfer of mass and momentum across the walls is generally unknown. However, from the comparison of both methods in Fig. 5 it appears that the technique describing the contraction of the slip stream by a sink will be sufficiently accurate for blockage ratios A_p/A_w below 10–15%.

Compressible Slip Stream

Compressible slip stream is described by the set of equations[11,12]

Station $0 \rightarrow 1$

$$A_0\rho_0 v_0 = A_p\rho_1 v_1 \tag{56}$$

$$\frac{v_0^2}{2} + \frac{\gamma}{\gamma-1}\frac{p_0}{\rho_0} = \frac{v_1^2}{2} + \frac{\gamma}{\gamma-1}\frac{p_1}{\rho_1} \tag{57}$$

$$p_0/\rho_0^\gamma = p_1/\rho_1^\gamma \tag{58}$$

Station $1 \rightarrow 2$

$$\rho_1 v_1 = \rho_2 v_2 \tag{59}$$

$$p_1 + \rho_1 v_1^2 + T/A_p = p_2 + \rho_2 v_2^2 \tag{60}$$

$$\frac{v_1^2}{2} + \frac{\gamma}{\gamma-1}\frac{p_1}{\rho_1} + \frac{P}{A_p\rho_1 v_1} = \frac{v_2^2}{2} + \frac{\gamma}{\gamma-1}\frac{p_2}{\rho_2} \tag{61}$$

Station $2 \rightarrow 3$

$$A_p\rho_2 v_2 = A_3\rho_3 v_3 \tag{62}$$

$$\frac{v_2^2}{2} + \frac{\gamma}{\gamma-1}\frac{p_2}{\rho_2} = \frac{v_3^2}{2} + \frac{\gamma}{\gamma-1}\frac{p_3}{\rho_3} \tag{63}$$

$$p_2/\rho_2^\gamma = p_3/\rho_3^\gamma \tag{64}$$

Far-field conditions

$$p_3 = p_0 \tag{65}$$

$$T = A_p\rho_1 v_1(v_3 - v_0) \tag{66}$$

Here, A_p, v_0, p_0, ρ_0, T, and P are expected to be known, and A_0, A_3, v_1, v_2, v_3, p_1, p_2, p_3, ρ_1, ρ_2, and ρ_3 are expected to be unknown.

From Eqs. (57), (61), and (63), the power added to the stream is

$$P = A_p\rho_1 v_1(v_3^2/2 - v_0^2/2 + \Delta i) \tag{67}$$

where

$$\Delta i = i_3 - i_0 = [\gamma/(\gamma-1)](p_3/\rho_3 - p_0/\rho_0) \tag{68}$$

is the increase of the slip-stream enthalpy, which does not contribute to the production of thrust. If the process is isentropic

$$p_1/\rho_1^\gamma = p_2/\rho_2^\gamma \tag{69}$$

then from Eqs. (58), (64), and (65)

$$\rho_3 = \rho_0 \tag{70}$$

and $\Delta i = 0$. In that case from Eqs. (66) and (67)

$$P = \tfrac{1}{2}(v_0 + v_3)T \tag{71}$$

and, substituting in Eq. (22)

$$\eta = 2v_0/(v_0 + v_3) = \eta_{id} \tag{72}$$

as for the incompressible slip stream, compare Eqs. (49) and (50).

The change of variables across the disk, which is treated as a discontinuity, can be established from Eqs. (59–61) using a procedure similar to that for a normal shock,[13] modified for the presence of the thrust and power terms. The difference of the velocities upstream and downstream of the propeller disk is obtained from Eqs. (59) and (60) as

$$v_1 - v_2 = \frac{p_2}{\rho_2 v_2} - \frac{p_1}{\rho_1 v_1} - \frac{T}{A_p \rho_1 v_1} \tag{73}$$

Because mechanical energy is added to the stream at the disk, we have to consider two critical velocities: c_{1*} upstream and c_{2*} downstream of the disk. The squares of these velocities are, with the help of Eqs. (57) and (61)

$$c_{1*}^2 = \frac{2\gamma}{\gamma+1}\frac{p_1}{\rho_1} + \frac{\gamma-1}{\gamma+1}v_1^2 = \frac{2\gamma}{\gamma+1}\frac{p_0}{\rho_0} + \frac{\gamma-1}{\gamma+1}v_0^2 \tag{74}$$

$$c_{2*}^2 = \frac{2\gamma}{\gamma+1}\frac{p_2}{\rho_2} + \frac{\gamma-1}{\gamma+1}v_2^2 = c_{1*}^2 + 2\frac{\gamma-1}{\gamma+1}\frac{P}{A_p\rho_1 v_1} \tag{75}$$

From Eqs. (74) and (75) the ratios p_1/ρ_1 and p_2/ρ_2 can be evaluated in terms of c_{2*} and substituted in Eq. (73). This gives

$$(v_1 - v_2)[c_{2*}^2/(v_1 v_2) - 1] = \nu \tag{76}$$

or

$$v_2^2 - (c_{2*}^2/v_1 + v_1 + \nu)v_2 + c_{2*}^2 = 0 \tag{77}$$

where

$$\nu = \frac{2}{\gamma+1}\left[\gamma T - (\gamma-1)\frac{P}{v_1}\right]\frac{1}{A_p\rho_1 v_1} \tag{78}$$

If $P = T = 0$, then $\nu = 0$ and also $c_{1*} = c_{2*} = c_*$. In this case Eq. (76) provides either continuity $v_2 = v_1$, or Prandtl's shock wave relationship $v_1 v_2 = c_*^2$. The latter is relevant only if $v_1/c_* > 1$. For a subcritical v_1, the smaller root of Eq. (77)

$$v_2 = \tfrac{1}{2}(c_{2*}^2/v_1 + v_1 + \nu) - \tfrac{1}{2}\sqrt{(c_{2*}^2/v_1 + v_1 + \nu)^2 - 4c_{2*}^2} \tag{79}$$

is thus the one to be chosen.

From Eqs. (78) and (22) it follows that ν will be positive if

$$\eta_{id} \geq \eta > [(\gamma-1)/\gamma]v_0/v_1$$

In this case the discriminant of Eq. (79) will satisfy

$$(c_{2*}^2/v_1 + v_1 + \nu)^2 - 4c_{2*}^2 > (c_{2*}^2/v_1 - v_1 + \nu)^2 > 0 \tag{80}$$

The direction of variation of quantities across the disk, as obtained from Eqs. (79), (80), (59), and (73), are such that

$$v_2 < v_1, \qquad \rho_2 > \rho_1, \qquad p_2 > p_1 + T/A_p$$

Calculations confirm that the corresponding entropy increment

$$s_2 - s_1 = [R/(\gamma-1)]\ln[(p_2/p_1)(\rho_1/\rho_2)^\gamma]$$

is positive as one should expect.[14]

Numerical solutions of the slip-stream equations (56–66) are provided by an iterative procedure, consisting of successive sweeps through stations 0, 1, 2, and 3. Since A_0 and A_3 appear only in Eqs. (56) and (62), they need not be directly involved in the solution process. In the first sweep, the incompressible-flow values [see Eqs. (46–48)]

$$v_1 = \tfrac{1}{2}(1+\Omega)v_0, \qquad v_3 = \Omega v_0 \tag{81}$$

are used as the initial guesses.

Station 0 → 1

First, the mass flux density is evaluated from Eq. (66):

$$j = \rho_1 v_1 = \frac{T}{A_p(v_3 - v_0)} \tag{82}$$

Combining Eqs. (57), (58), and (82), v_1 can be calculated as a root of

$$f(v_1) = v_1^2 - v_0^2 + [2\gamma/(\gamma-1)](p_0/\rho_0) \times [(j/\rho_0)^{\gamma-1}v_1^{1-\gamma} - 1] = 0 \tag{83}$$

using Newton's method. Since f has a local minimum at

$$v_{1m} = [\gamma(p_0/\rho_0)(j/\rho_0)^{(\gamma-1)}]^{1/(\gamma+1)} \tag{84}$$

Eq. (83) has a solution only if

$$f(v_{1m}) \leq 0 \tag{85}$$

The limit $f(v_{1m}) = 0$ determines the maximum j for which the solution still exists. It can be shown that

$$\max j < j_* = \rho_0(c_{1*}/c_0)^{2(\gamma-1)}c_{1*}$$

where c_0 is the upstream velocity of sound and j_* is the critical mass flux density corresponding to $v_1 = c_{1*}$.

The rest of the computational sweep is easy. Knowing j and v_1, the corresponding values of ρ_1 and p_1 are obtained from Eqs. (82) and (58), respectively.

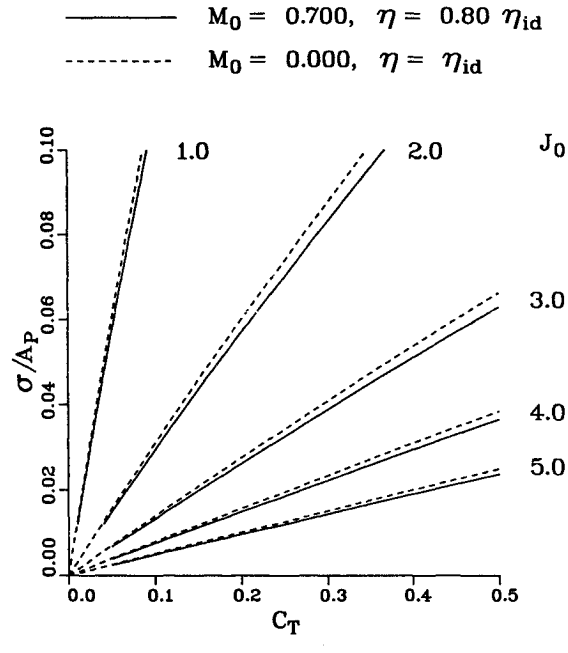

Fig. 6 Sink strength for compressible and incompressible slipstreams.

Station 1 → 2

The velocity behind the propeller plane v_2 is evaluated from Eq. (79), where c_{2*} and ν are calculated from Eqs. (75) and (78), respectively. The value of ρ_2 is obtained from Eqs. (59) and (82), and p_2 from Eq. (75).

Station 2 → 3

The values of p_3 and ρ_3 are obtained successively from Eqs. (65) and (64), and v_3 from Eq. (63).

The compressible-flow values ρ_1, v_1, and v_3 are now used to check if Eq. (66) is satisfied, subject to some accuracy criterion (e.g., $<T/10^5$). If not, j is slightly decreased and a new sweep, starting with Eq. (83), is initiated. The subsequent updates of j are obtained by interpolation or extrapolation, targeting on the prescribed thrust while restricting the possible overshoots of j by the condition described by Eqs. (85) and (84).

Once a converged result has been obtained, the cross-sectional areas far upstream and downstream are evaluated from Eqs. (56) and (62) as

$$A_0 = A_p j/(\rho_0 v_0), \qquad A_3 = A_p j/(\rho_3 v_3) \tag{86}$$

and substituted in Eq. (34) to obtain σ.

An example of evaluated sink strengths is given in Fig. 6. The values of σ/A_p for an incompressible slip stream (broken lines) collapse to the single curve of Fig. 4, when plotted as a function of η_{id}. It is seen that the compressible-flow values of σ are a little less than the incompressible ones. Similar calculations show that the effect of compressibility becomes more significant as η decreases. However, for high-efficiency propellers tested at $M_0 < 0.8$ the incompressible stream approximation of σ is adequate.

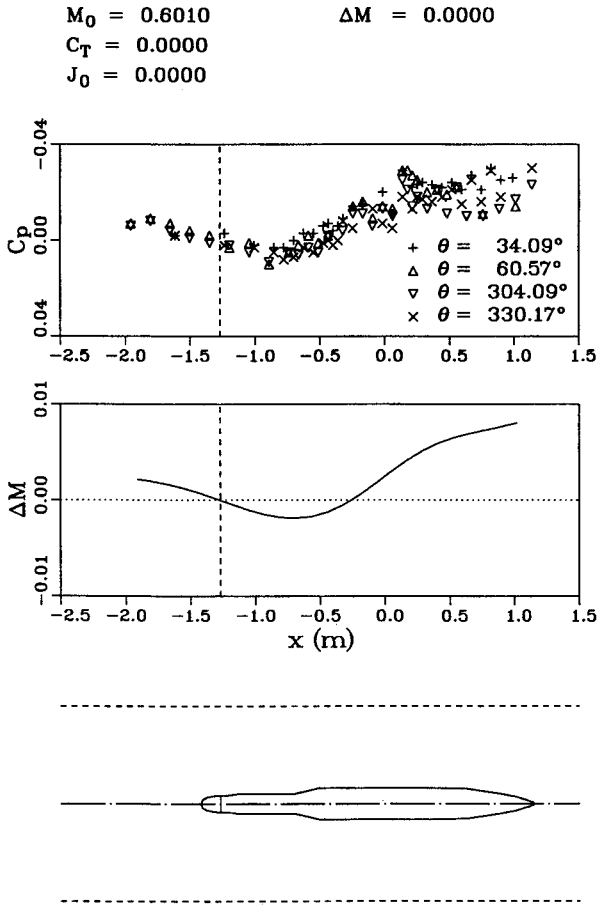

Fig. 7 Wall pressures and axial Mach correction; without propeller.

Propeller Test Example

The example given here is merely illustrative rather than representative of the variety of situations that were encountered in the wind-tunnel study[15] of the de Havilland four-, six-, and eight-bladed propfans.

The test stand (Fig. 1) mounted on the half-model balance in the sidewall, was designed so that the measured data would largely represent "isolated" propeller data, free from wing interference. The nacelle, which contained a torque sensor in its forebody and an electric motor drive in its aft cowling, would still interact with the slip stream.

Porosity of the perforated walls of the 1.5 × 1.5 m test section of the IAR Blowdown Wind Tunnel was set at 4%, which turned out to be an appropriate choice for the test. Wall pressure measurements were made using six static pressure tubes, but only four of them, two on the outboard sidewall (opposite to the mounting strut) and one on the top and bottom wall each were used to evaluate wall interference.

Figures 7 and 8 show the measured wall pressures at $M_0 = 0.601$ and the axial Mach number corrections evaluated by the described correction method, for a nacelle without and with a (running) propeller. The propeller was tested at Reynolds number 5×10^6/m.

The maximum radius of the nacelle cowling was 0.076 m, and the radius of the four-bladed propeller was 0.305 m, yielding wind-tunnel blockage ratios of 0.8 and 12.6%, respectively.

Without a propeller (Fig. 7) the observed Mach number correction is mainly due to flow nonuniformity in the empty test section and the blockage effect of the nacelle. The far field of the nacelle was represented by a sink-source body of the same length and volume. The effect of the strut, attaching the propeller rig to the sidewall, has not been accounted for.

For a propeller operating at 5000 rpm (Fig. 8) there is an additional wall interference effect induced by the sink term representing the corresponding contraction of the slip stream.

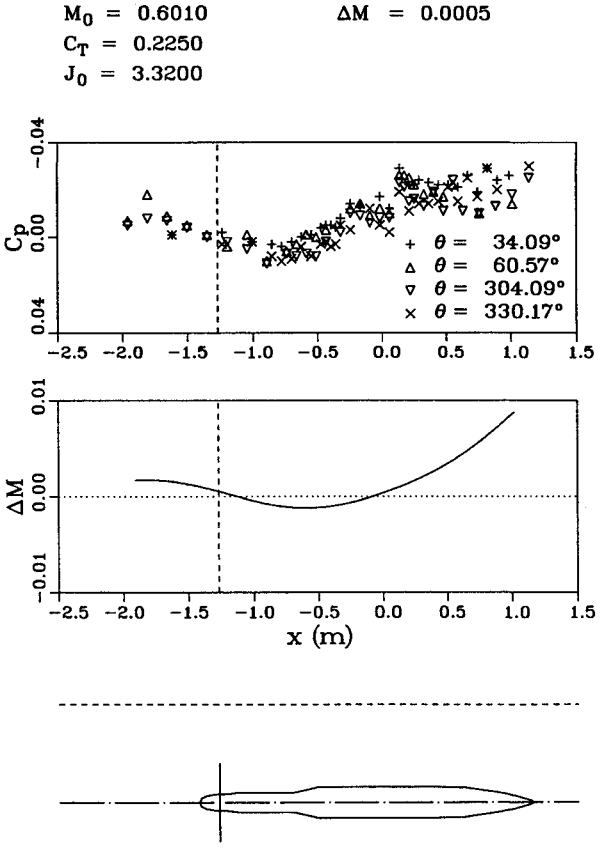

Fig. 8 Wall pressures and axial Mach correction; with propeller.

The strength of the sink was obtained from the measured C_T and J_0 using the incompressible-flow approximation.

Although the differences of the wall pressures in the two cases are barely discernible, there is some difference in the calculated ΔM curves. At the propeller location (vertical broken line), $\Delta M = 0.0000$ with power off and $\Delta M = 0.0005$ with power on. From the repeat runs it appeared that the accuracy of ΔM was about ± 0.0002.

It is evident that by just evaluating ΔM along the wind-tunnel axis the method has not been utilized to its full capacity. Using Eqs. (9) and (21), ΔM can be calculated anywhere inside the (cylindrical) flow domain shown in Fig. 2. The variations of ΔM in the propeller plane would be of interest when evaluating propeller performance from flowfield measurements,[16] but first the influence of the boundary data interpolation at the upstream and downstream ends [see Eqs. (13)] would have to be assessed. By integrating the irrotational flow conditions, the radial component of wall interference velocity can also be evaluated.[4]

Concluding Remarks

A one-component correction method has been proposed for propellers (and propfans) tested at subsonic speeds in perforated wall wind tunnels. The streamwise component of the wall interference velocity at the wind-tunnel boundaries is derived from the static pressure tube measurements and the far field of the propeller in free air. The radial contraction of the propulsive stream tube is modeled in the far field by a sink term, whose strength and location are evaluated from the measured thrust and power using axial momentum theory. The axial values of the wall interference velocity are then obtained from the Fourier solution of a Dirichlet problem inside a cylindrical flow domain.

A comparison with the Glauert correction[2] for incompressible flow in a closed-wall wind tunnel shows a good agreement for blockage ratios (propeller disk area to wind-tunnel cross section) up to about 10%. For higher blockage ratios the method described here provides a sink strength that underestimates the closed-wall corrections according to Glauert. Based on the conservation laws, Glauert's approach is the more rigorous one, but unfortunately, cannot be applied to ventilated-wall wind tunnels, where fluxes of mass and momentum across the walls are generally unknown. Evidently, a sink strength that provides a perfect agreement with Glauert's theory in the closed-wall case could also be used to correct propeller tests in the perforated-wall case, but justifiably only at small wall porosities. This combination of the two methods, which could provide a viable alternative to correcting low speed wind-tunnel tests of propellers at high blockage ratios, has not been further explored.

In the derivation of the subsonic sink strength a complete overview of the compressible-flow theory for the propeller disk has been given. Of main concern was the possible existence of two different solutions for the compressible slip-stream equations, as described by Delano and Crigler.[12] However, postprocessing of the published results from the same reference[12] has shown that the solution in which flow accelerates across the propeller disk into supersonic speeds is, in analogy to an expansion shock, accompanied by a decrease in entropy. A physically meaningful solution,[14] providing a nonnegative entropy increment, decelerates flow across the disk and exists for a range of efficiencies below the ideal (Froude) efficiency. The corresponding slip-stream velocities, obtained numerically by Newton's method, were found to provide a sink strength that is somewhat less than that obtained by an incompressible-flow approximation.

In the IAR Blowdown Wind-Tunnel test section, whose perforated walls with 60-deg slanted holes were set at 4% openness ratio, the blockage correction evaluated for the de Havilland propeller tests was found to be rather small, not significantly influencing the measured propeller performance characteristics.[15] The source strength, used to model the propeller far field in this low-correction case, was the one obtained from the incompressible slip-stream theory. The obtained result indicates that perforated walls are indeed suitable for high-speed propeller testing, now that the corresponding wall interference effect can also be quantified.

Appendix: Fourier Solution

The solution of the boundary value problem described by Eqs. (13) can be obtained as

$$f_n(\xi, \rho) = f_{n1}(\xi, \rho) + f_{n2}(\xi, \rho)$$

where f_{n1} and f_{n2} are the solutions of the separate problems

$$D_n f_{n1}(\xi, \rho) = 0, \qquad 0 < \xi < s, \qquad 0 \le \rho < r$$

$$f_{n1}(\xi, r) = \hat{f}_n(\xi), \qquad 0 \le \xi \le s$$

$$f_{n1}(0, \rho) = 0, \qquad 0 \le \rho < r$$

$$f_{n1}(s, \rho) = 0, \qquad 0 \le \rho < r$$

$$D_n f_{n2}(\xi, \rho) = 0, \qquad 0 < \xi < s, \qquad 0 \le \rho < r$$

$$f_{n2}(\xi, r) = 0, \qquad 0 < \xi < s$$

$$f_{n2}(0, \rho) = \hat{f}_n(0)(\rho/r)^n, \qquad 0 \le \rho \le r$$

$$f_{n2}(s, \rho) = \hat{f}_n(s)(\rho/r)^n, \qquad 0 \le \rho \le r$$

First problem: separating the variables as

$$f_{n1}(\xi, \rho) = X_1(\xi) R_1(\rho)$$

we obtain, using the differential operator (11)

$$\frac{X_1''}{X_1} = -\frac{R_1''}{R_1} - \frac{R_1'}{\rho R_1} + \frac{n^2}{\rho^2} = -\mu^2$$

where $-\mu^2$ is a constant (selected to be negative). The eigenvalue problem

$$X_1'' + \mu^2 X_1 = 0, \qquad 0 < \xi < s$$

$$X_1(0) = X_1(s) = 0$$

obtained from the first differential equation and the homogeneous boundary conditions, is satisfied for the eigenfunctions $\sin \mu_k \xi$, where μ_k is given by the first of Eqs. (15). Since a nonsingular solution of the second differential equation

$$\rho^2 R_1'' + \rho R_1' - (\mu^2 \rho^2 + n^2) R_1 = 0, \qquad 0 \le \rho < r$$

is

$$R_1 = F[I_n(\mu\rho)/I_n(\mu r)]$$

where F is an arbitrary constant, we can construct f_{n1} as

$$f_{n1}(\xi, \rho) = \sum_{k=1}^{\infty} F_{n,k} \frac{I_n(\mu_k \rho)}{I_n(\mu_k r)} \sin \mu_k \xi$$

The substitution in the nonhomogeneous boundary condition leads to the Fourier sine series

$$\sum_{k=1}^{\infty} F_{n,k} \sin \mu_k \xi = \hat{f}_n(\xi), \qquad 0 \le \xi \le s$$

so that $F_{n,k}$ has to be chosen as described by Eq. (16).

Second problem: using

$$f_{n2}(\xi, \rho) = X_2(\xi)R_2(\rho)$$

we obtain

$$\frac{X_2''}{X_2} = -\frac{R_2''}{R_2} - \frac{R_2'}{\rho R_2} + \frac{n^2}{\rho^2} = \nu^2$$

where ν^2 is a constant (selected to be positive). The eigenvalue problem

$$\rho^2 R_2'' + \rho R_2' + (\nu^2\rho^2 - n^2)R_2 = 0, \qquad 0 \le \rho < r$$

$$R_2(r) = 0$$

is satisfied for the nonsingular functions $J_n(\nu_{n,k}\rho)$, where $\nu_{n,k}$ is given by the second of Eqs. (15). Since the general solution of

$$X_2'' - \nu^2 X_2 = 0, \qquad 0 < \xi < s$$

is

$$X_2 = P\frac{\sinh \nu(s - \xi)}{\sinh \nu s} + Q\frac{\sinh \nu\xi}{\sinh \nu s}$$

where P and Q are arbitrary constants, we can construct f_{n2} as

$$f_{n2}(\xi, \rho) = \sum_{k=1}^{\infty}\left[P_{n,k}\frac{\sinh \nu_{n,k}(s - \xi)}{\sinh \nu_{n,k}s} + Q_{n,k}\frac{\sinh \nu_{n,k}\xi}{\sinh \nu_{n,k}s}\right] \times J_n(\nu_{n,k}\rho)$$

The substitution in the nonhomogeneous boundary conditions leads to the Fourier–Bessel series

$$\sum_{k=1}^{\infty} P_{n,k}J_n(\nu_{n,k}\rho) = \hat{f}_n(0)(\rho/r)^n, \qquad 0 \le \rho \le r$$

$$\sum_{k=1}^{\infty} Q_{n,k}J_n(\nu_{n,k}\rho) = \hat{f}_n(s)(\rho/r)^n, \qquad 0 \le \rho \le r$$

From the orthogonality properties of the Bessel functions it follows that the coefficients $P_{n,k}$ and $Q_{n,k}$ have to satisfy Eqs. (17).

Acknowledgments

This work has been carried out under the Project "Wind Tunnel Wall Interference," in support of the collaborative research program "Wing/Propeller Slip Stream Interactions" between de Havilland, Inc. and the Institute for Aerospace Research. The author wishes to thank V. D. Nguyen and L. H. Ohman of IAR for their generous cooperation and for sharing their experimental data. The suggestions and personal notes of R. H. Wickens, formerly of IAR, were most helpful in the derivation of the propeller far field and are also gratefully acknowledged.

References

[1]"Aerodynamics and Acoustics of Propellers," *Proceedings of the Fluid Dynamics Symposium*, Feb. 1985 (AGARD CP-366).

[2]Glauert, H., *The Elements of Aerofoil and Airscrew Theory*, 2nd ed., Cambridge Univ. Press, Cambridge, England, UK, 1959, pp. 199–207, 222–226.

[3]Capelier, C., Chevallier, J. P., and Bouniol, F., "Nouvelle Méthode de Correction des Effets de Parois en Courant Plan," *La Recherche Aérospatiale*, Jan.–Feb. 1978, pp. 1–11.

[4]Mokry, M., "Subsonic Wall Interference Corrections for Finite-Length Test Sections Using Boundary Pressure Measurements," *Proceedings of the Fluid Dynamics Panel Specialists' Meeting*, 1982, pp. 10.1–10.15 (AGARD CP-335).

[5]Rizk, M. H., and Smithmeyer, M. G., "Wind-Tunnel Wall Interference Corrections for Three-Dimensional Flows," *Journal of Aircraft*, Vol. 19, No. 6, 1982, pp. 465–472.

[6]Ashill, P. R., and Weeks, D. J., "A Method for Determining Wall-Interference Corrections in Solid-Wall Tunnels from Measurements of Static Pressure at the Walls," *Proceedings of the Fluid Dynamics Panel Specialists' Meeting*, 1982, pp. 1.1–1.12 (AGARD CP-335).

[7]Kraft, E. M., Ritter, A., and Laster, M. L., "Advances at AEDC in Treating Transonic Wind Tunnel Wall Interference," *ICAS Proceedings 1986*, pp. 748–769.

[8]Mokry, M., and Ohman, L. H., "Application of the Fast Fourier Transform to Two-Dimensional Wind Tunnel Wall Interference," *Journal of Aircraft*, Vol. 17, No. 6, 1980, pp. 402–408.

[9]Vallentine, H. R., *Applied Hydrodynamics*, Butterworths, London, 1967, pp. 244–246.

[10]Wright, R. H., "The Effectiveness of the Transonic Wind Tunnel as a Device for Minimizing Tunnel-Boundary Interference for Model Tests at Transonic Speeds," AGARD Rept. 294, March 1959.

[11]Vogeley, A. W., "Axial-Momentum Theory for Propellers in Compressible Flow," NACA TN 2164, July 1951.

[12]Delano, J. B., and Crigler, J. L., "Compressible-Flow Solutions for the Actuator Disk," NACA RM L53A07, March 1953.

[13]Landau, L. D., and Lifshitz, E. M., *Fluid Mechanics*, Pergamon, Oxford, England, UK, 1959, pp. 325–333.

[14]Küchemann, D., and Weber, J., *Aerodynamics of Propulsion*, McGraw–Hill, New York, 1953, pp. 9–37.

[15]Nguyen, V. D., and Ohman, L. H., "Wind Tunnel Investigation of De Havilland 4 and 6-Bladed Propellers and 8-Bladed Propfans at Mach Numbers 0.35 to 0.72," Inst. for Aerospace Research, National Research Council of Canada, LTR-HA-5x5/0223, Ottawa, Canada, June 1993.

[16]Ohman, L. H., Nguyen, V. D., and Barber, D. J., "Probe Interference on Flow Measurements in Propeller near Slip Stream," *Journal of Aircraft*, Vol. 32, No. 4, 1995, pp. 887, 888.